Geophysical Research Letters

RESEARCH LETTER
10.1029/2022GL102422

Key Points:

- Three decades of repeat hydrographic sections reveal decreasing density stratification in the deep and abyssal layers of the Southern Ocean
- South of 60°S, N^2 has reduced by 6% per decade in the ocean below 4,000 m, with a peak reduction rate of 15% per decade at 4,800 m
- The decreasing stratification is found along the pathway of Antarctica Bottom Water and its vertical structure depends on the topography of basin boundaries

Supporting Information:

Supporting Information may be found in the online version of this article.

Correspondence to:

S. Tan,
shuwent@ldeo.columbia.edu

Citation:

Tan, S., & Thurnherr, A. M. (2023). On the global decrease in the deep and abyssal density stratification along the spreading pathways of Antarctic Bottom Water since the 1990s. *Geophysical Research Letters*, *50*, e2022GL102422. https://doi.org/10.1029/2022GL102422

Received 6 DEC 2022
Accepted 19 APR 2023

On the Global Decrease in the Deep and Abyssal Density Stratification Along the Spreading Pathways of Antarctic Bottom Water Since the 1990s

Shuwen Tan[1] and Andreas M. Thurnherr[1]

[1]Lamont-Doherty Earth Observatory, Columbia University, Palisades, NY, USA

Abstract The density stratification in the ocean is directly related to the diapycnal mixing, which drives the abyssal cell of the Meridional Overturning Circulation (MOC). It is important to understand how stratification has been changing in the world's deep and abyssal oceans under climate change. Using repeat hydrographic data obtained since the 1990s, we find a decreasing stratification associated with changes in the source Antarctica Bottom Water (AABW) properties in its formation basins as well as in basins along its dispersal pathways. Averaged south of 60°S, the squared buoyancy frequency N^2 shows a negative trend of −6% per decade in waters deeper than 4,000 m. The observed decadal reduction in stratification is associated with large spatial variability, especially in the Southern Ocean basins with multiple AABW sources. Additionally, there are also significant differences between neighboring basins that are related to the blocking effect of topography.

Plain Language Summary Cold and dense Antarctica Bottom Water (AABW) forms near the coastline of Antarctica, sinks to the ocean bottom, moves northward in deep branches of the Meridional Overturning Circulation, becomes lighter through mixing, and eventually upwells to shallower depths. The AABW properties change under the changing climate. Repeat hydrography sections occupied approximately once per decade since the 1990s have revealed continuously warming and freshening of the AABW. In many regions of the ocean, the warming and freshening trends are strongest at the bottom. This causes a decrease in the vertical gradient of density, namely stratification. As the level of mixing is strongly related to stratification, it is important to quantify its trend and understand its spatial structure. We quantify the trend in stratification globally and find a reduction in stratification in the Southern Ocean and along the spreading pathways of the AABW at lower latitudes.

1. Introduction

The Meridional Overturning Circulation (MOC) plays a key role in the Earth's climate by uptaking and redistributing heat and carbon (Marshall & Speer, 2012). Its abyssal branch, fed by Antarctic Bottom Water (AABW), spreads northward and upwells across isopycnals by turbulent mixing (Marshall & Speer, 2012; Munk, 1966; Stommel & Arons, 1959). Carried out in the 1990s, the World Ocean Circulation Experiment (WOCE) occupied ship-based Conductivity-Temperature-Depth (CTD) sections that cross all oceans around the globe. The hydrographic sections were repeated roughly every decade by the Climate Variability and Predictability (CLIVAR) program through the 2000s and the Global Ocean Ship-Based Hydrographic Investigations Program (GO-SHIP) since the 2010s (Talley et al., 2016). The collective high-quality, full-depth, hydrographic profiles have unveiled a warming (Desbruyères et al., 2016; Purkey & Johnson, 2010; Purkey et al., 2019), freshening (Menezes et al., 2017; Purkey & Johnson, 2013), and contracting (Purkey & Johnson, 2012; van Wijk & Rintoul, 2014) trend in AABW since the 1990s. The trend has not only been found in the formation basins of AABW, but also in downstream basins of the deep branches of the MOC. The warming and freshening trends in AABW, however, are not vertically uniform, which induces changes in the vertical density gradient, or stratification. Different warming and freshening rates in the AABW and the overlying North Atlantic Deep Water (NADW) can also cause changes in the stratification (Johnson et al., 2020).

Changes in stratification affect the internal wave characteristics, wave-wave interactions, breaking of internal waves, and turbulent mixing, thereby influencing the diapycnal transport and distribution of heat, freshwater, dissolved gas, and biochemical tracers (Garrett & Kunze, 2007; Gregg, 1989; Legg, 2021; MacKinnon et al., 2017; Whalen et al., 2020). In the deep and abyssal oceans, a changing stratification has important implications for the MOC. Considering the energetics of the system, the closure of the abyssal limb of the MOC requires

turbulent mixing to work against the density stratification to transform the dense abyssal waters into lighter waters (Munk & Wunsch, 1998). As a result, decadal trends in the density stratification of the deep ocean are expected to affect the upwelling rate and, consequently, the strength of the MOC. Deep ocean stratification also affects the transport of overflows in deep ocean passages through hydraulic control (Pratt & Whitehead, 2007; Whitehead, 1998). Examples of hydraulically controlled overflows along the pathways of the abyssal limb of the MOC include the Vema Channel overflow that provides a conduit for bottom water to enter the Brazil basin (BB) from the Argentine basin (Tarakanov et al., 2020), overflows in a Fracture Zone Valley that runs from the deep BB to the crest of the Mid-Atlantic Ridge (Clément et al., 2017; Thurnherr et al., 2005), as well as the Samoan Passage overflow that connects the Southwest Pacific basin (PB) with the PB (Alford et al., 2013). These considerations imply that knowledge of trends in the deep and abyssal ocean stratification is required for understanding changes in the MOC, and the trends are also useful on their own as indicators for climate change.

In the upper 2,000 m of the ocean, surface-intensified warming has caused a positive stratification trend of 0.9% per decade since the 1960s (Li et al., 2020). In contrast with the upper ocean, recent studies report a bottom-intensified warming trend in many regions in the Southern Hemisphere associated with changes in the AABW properties at least since the 1990s (Purkey et al., 2019), implying a decrease in stratification in the deep ocean. Johnson et al. (2020) estimate a reduction rate of the stratification of 1% per decade in the BB from the difference between the warming rate averaged within the AABW layer and the warming rate at one depth in the overlying NADW. Note that this is a bulk estimate for the stratification change between AABW and NADW and does not resolve any vertical structure. Zhang et al. (2021), on the other hand, provide a vertical profile of the stratification trend for the Southwest PB and estimate a mean stratification reduction rate of 12% per decade for water below $\Theta = 0.8°C$ (Θ is conservative temperature). Apart from these regional studies, stratification changes in the global ocean have not yet been quantified, and the vertical structure of the changes and the lateral variability between ocean basins have never been investigated. In this paper, we synthesize hydrographic data from full-depth repeat sections and provide the first global quantification of stratification changes since the 1990s.

2. Data and Methods

2.1. Repeat Hydrography Sections

The temperature, salinity, and pressure data used in this study come from the GO-SHIP Easy Ocean *reported* product (Katsumata et al., 2022), which is the uninterpolated hydrographic data product from the ship-based CTD sections repeated by three global-scale surveys started in the 1990s: WOCE, CLIVAR, and GO-SHIP, as of September 2021. Along each section, CTD profiles were taken typically 55 km apart, from the sea surface to a depth of 10–20 m from the bottom, and were binned into 1 or 2 dbar pressure bins. The accuracy of the data follows the GO-SHIP standard (Hood et al., 2010): 0.002°C for temperature, 0.002 g kg^{-1} for Absolute Salinity under TEOS-10 (McDougall & Barker, 2011), and 3 dbar for pressure. The squared buoyancy frequency N^2 was calculated from those profiles (see Section 2.2) and then interpolated to a uniform 0.1° horizontal grid using the GO-SHIP Easy Ocean *gridded* product generation software.

2.2. Calculating the Stratification Trend

As a measure of stratification, the squared buoyancy frequency N^2 was calculated from the vertical gradient of density:

$$N^2(z) = -\frac{g}{\rho_0}\frac{\partial \rho}{\partial z}, \tag{1}$$

where g is the gravity acceleration as a function of latitude and pressure, $\frac{\partial \rho}{\partial z}$ was estimated from the slope of a linear least-square fit in 40 m-thick layers with ρ being the potential density referenced to the mean pressure in the layer, ρ_0 is the corresponding mean potential density. This filters out spikes in density gradients due to the instrument noise and transient processes such as turbulent overturns in a similar manner to the approach used by Zhang et al. (2021), who applied a 40-dbar half-width Hanning filter to temperature and salinity profiles at a resolution of 1-dbar and then interpolated the filtered profiles onto a vertical 40-dbar pressure grid.

At each depth, we then estimated the trend in N^2 from the time series using a linear least-square fit. In order to reduce the effects of high-frequency variability while retaining the spatial structure along each section, the

fine-grid N^2 trend of 0.1° by 40 m was averaged within grids of 5° by 400 m. The number of degrees of freedom (DOF) for each grid was estimated accounting for both the horizontal and vertical decorrelation length scales of 163 km and 80 m, respectively. The former was taken from Purkey and Johnson (2010) and the latter was approximated by the mean of the vertical decorrelation length scale for all sections at all depths. The vertical decorrelation length scale was estimated following Purkey and Johnson (2010) by first estimating the lagged auto-correlation of each vertically detrended N^2 changing rate, and then doubling the maximum of the integral of the lagged auto-correlation. The mean vertical decorrelation length scale over the entire water column is similar to the mean in waters deeper than 2,000 m. The confidence interval for the grid-mean was estimated by assuming a Student's t distribution. Global and basin mean N^2 trends were calculated and standard error-propagation methods were used to estimate the confidence interval.

We also calculated the N^2 trends in density space, using σ_4, the potential density anomaly with a reference pressure of 4,000 dbar calculated using the TEOS-10 toolbox (McDougall & Barker, 2011). At each station, N^2 for each occupation was linearly interpolated onto a 0.005 kg m^{-3} grid, and then the trend was calculated for each grid point. N^2 trends were then averaged within grids of 5° by 0.025 kg m^{-3}. For each occupation, the number of DOF within each grid cell was estimated by dividing the area of the density layer within the 5° grid by the horizontal and vertical decorrelation lengths. The confidence interval was estimated by assuming a Student's t distribution with the number of DOF for each grid approximated by the lowest value of all occupations.

3. Results

3.1. Decreasing Stratification in the AABW

By computing the N^2 trend for repeat hydrographic sections over the global ocean (Figure 1a), we find that waters below 2,000 m show patches of significantly negative N^2 trends throughout basins in the Southern Hemisphere (Figures 1b and 2). Furthermore, we notice a bottom-reaching and isopycnal-following negative N^2 trend in many Southern Ocean basins. This is particularly evident in the Amundsen-Bellingshausen basin in the Pacific sector of the Southern Ocean (sections P16, P17E, and P18) and in the Australian-Antarctic basin (AAB) in the Indian sector of the Southern Ocean (sections I08S-I09N and I09S). Bottom-intensified warming and freshening have been observed in both basins (Desbruyères et al., 2016; Johnson et al., 2008; Menezes et al., 2017; Purkey & Johnson, 2013; Purkey et al., 2019). The coherent negative trend following the deep isopycnals suggests that the stratification change is related to decadal changes in the AABW.

In order to quantify the global deep and abyssal ocean stratification changes, we average the N^2 trends from repeat sections (Figure 3a). The Southern Hemisphere average is generally negative below 2,500 m, while the Northern Hemisphere average is generally positive above 5,500 m and has a much larger variability. When averaged over profiles south of 60°S, a much more consistent negative trend and tighter confidence intervals are found below 2,000 m, compared to the average of the entire Southern Hemisphere. Since AABW constitutes the highest percentage of abyssal waters in deep basins south of 60°S (Johnson, 2008), the result quantifies the global reduction of stratification in the AABW. The positive mean trend in the Northern Hemisphere above 5,500 m is possibly related to the cooling of the NADW (Desbruyères et al., 2017). We also estimate the relative change of N^2 by dividing the N^2 trend at each depth by the spatially averaged N^2 from the initial occupation of the repeat sections (Figure 3b). The average N^2 changes within the deep (2,000–4,000 m) and abyssal (≥4,000 m) layers south of 60° S are about −3% and −6% per decade, respectively (Table S1 in Supporting Information S1). Only the former value significantly differs from zero at the 95% confidence level. Despite the larger variability of N^2 trends below 4,000 m, the maximum reduction rate of about −15% per decade at 4,800 m is significantly different from zero. Below that depth, the averaged N^2 trend exhibits large variability, which is likely linked to the variability of seafloor depth in the AABW formation basins.

3.2. Decadal N^2 Trends by Basin

The N^2 trends estimated along repeat sections in Figures 1b and 2 not only show vertical variability but also show lateral variability between deep ocean basins. 33 basins divided by ocean ridges were identified by Purkey and Johnson (2010), and the repeat sections cross 28 of them (Figure 1a). Averaged N^2 trends for the 18 basins entirely or partially located in the Southern Hemisphere are shown in Figures S1 and S2 in Supporting Information S1, and the layer averages are listed in Table S2 in Supporting Information S1. In order to illustrate the spatial pattern

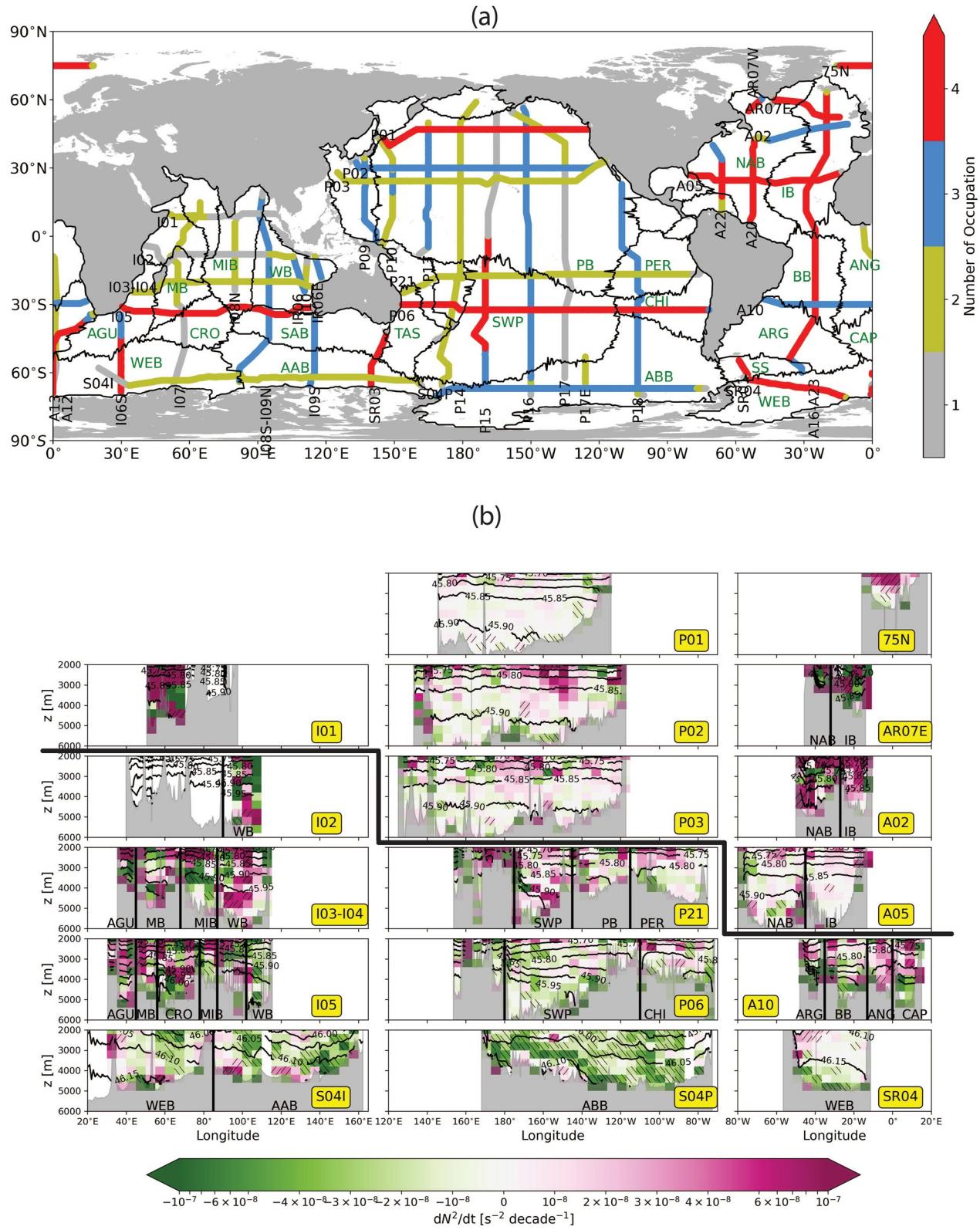

Figure 1.

of the decreasing stratification in AABW, we average N^2 trends across densities greater than $\sigma_4 = 45.95$ kg m^{-3} along repeat sections (Figure 4). This upper boundary of AABW is chosen to correspond to the isopycnal that separates the AABW from the overlying NADW in the Samoan Passage, which connects the Southwest PB with the PB at about 8°S (Carter et al., 2019; Cusack et al., 2019).

3.2.1. N^2 Trends in the Southern Ocean

Among the three southernmost basins, where AABW fills both deep and abyssal layers (Johnson, 2008), the decadal change in stratification appears to be very different. Significantly negative N^2 trends averaged for waters denser than $\sigma_4 = 45.95$ kg m^{-3} are found at most stations in the ABB and in the AAB (Figure 4). These negative N^2 trends are consistent with previous reports of the bottom-intensified decadal warming and/or freshening of waters in the following AABW formation regions: Ross Sea in the southwestern ABB and off the Adelie Land south of the AAB (Menezes et al., 2017; Purkey et al., 2019). In contrast, stratification changes in the Weddell–Enderby basin are dominated by very large variability, with a basin-averaged N^2 trend that does not significantly differ from zero. The depth-averaged N^2 trends show decreasing stratification averaged below 4,000 m in the western Weddell–Enderby basin (Figure S3 in Supporting Information S1), but no significant trends are detected when averaging across densities greater than $\sigma_4 = 45.95$ kg m^{-3}. On the other hand, negative N^2 trends averaged below $\sigma_4 = 45.95$ kg m^{-3} occur in the eastern part of the basin. Taken together, these observations suggest different changes in AABW properties from the two different sources in the Weddell–Enderby basin: the eastern formation region Prydz Bay, and the western formation region Weddell Sea (Solodoch et al., 2022). In fact, we find bottom-intensified warming and freshening trends between 50°E and 80°E of section S04I in the eastern Weddell-Enderby basin, both of which are associated with decreasing stratification (Figures S4 and S5 in Supporting Information S1). In contrast, bottom-intensified increasing trends in salinity are observed across section SR04 in the western Weddell-Enderby basin, which counteracts the effects of bottom-intensified warming on reducing stratification. In comparison, the stratification trends averaged over a lighter density layer of 45.7 kg m^{-3} $\leq \sigma_4 <$ 45.95 kg m^{-3} in all three basins show large variability and do not reveal any significant trends (Figures S2 and S3 in Supporting Information S1).

3.2.2. N^2 Trends Along the AABW Dispersal Pathway

Our analysis of stratification changes in basins away from AABW formation basins in the Southern Ocean shows that: (a) negative N^2 trends occur downstream of the formation basins along the pathway of AABW (blue arrows in Figure 4); (b) the vertical structure of the N^2 trends in downstream basins depends on the sill depths of the passages between the basins.

In the Pacific Ocean: AABW exits the ABB through the Eltanin fracture zone into the Southwest PB, follows the western boundary of the basin, and enters the PB through the Samoan Passage (Purkey et al., 2019). Along its path, AABW mixes with ambient waters and becomes lighter. As a result, waters denser than $\sigma_4 = 45.95$ kg m^{-3} only extend to about 20°N along section P14 in the west of the PB. The N^2 trend averaged below $\sigma_4 = 45.95$ kg m^{-3} shows a decreasing stratification along the path of AABW. The relative change of N^2 averaged across the Southwest PB is −23% per decade, which is about twice the estimate of −12% per decade for water below $\Theta = 0.8$°C from Zhang et al. (2021). The different procedures to estimate the trends are likely to contribute to the trend difference, as Zhang et al. (2021) calculated trends in $\log(N^2)$ before converting the trends into a percentage change, while we estimated the linear trends of N^2. The difference is possibly also due to a combination of the different layer-averaging choices, averaging over five repeat sections compared to three, and accounting for the effect of salinity change. In contrast to the pathway through the Samoan Passage, ABB-sourced abyssal waters denser than $\sigma_4 = 45.85$ kg m^{-3} are blocked from entering the Chile basin by the Chile Rise. Despite that, waters denser than $\sigma_4 = 45.8$ kg m^{-3}, which is typically deeper than 3,000 m in the Chile basin, show negative N^2 trends

Figure 1. (a) Approximate locations of Global Ocean Ship-Based Hydrographic Investigations Program Easy Ocean *reported* sections with section names. The vertical and lateral oriented section names demark meridional and zonal sections, respectively. The color shows how many times a segment of a section has been occupied as of September 2021. This figure is adapted from Figure 2b in Katsumata et al. (2022). 33 basins identified by Purkey and Johnson (2010) are outlined in black. Key basins are labeled with abbreviations in green: WEB (Weddell–Enderby basin), AAB (Australian-Antarctic basin), AGU (Agulhas–Mozambique basin), CRO (Crozet basin), SAB (South Australian basin), MB (Madagascar basin), MIB (mid-Indian basin), WB (Wharton basin), ABB (Amundsen-Bellingshausen basin), TAS (Tasman Sea), SWP (Southwest Pacific basin), CHI (Chile basin), PER (Peru basin), PB (Pacific basin), SS (Scotia Sea), ARG (Argentine basin), CAP (Cape basin), BB (Brazil basin), ANG (Angola basin), NAB (North Atlantic basin), IB (Iberian/Canary/Cape Verde basin). (b) dN^2/dt calculated within 5° × 400 m grids, with results that are significantly different from zero at the 95% confidence level crosshatched. Results are shown along zonal sections in the Indian Ocean (left), Pacific Ocean (middle), and Atlantic Ocean (right). The latitude of zonal sections in each subplot increases from the bottom up, and the subplots below the black step line show sections in the Southern Hemisphere. The bottom panel shows sections south of 60°S. Topography is shaded gray and basins divided by ocean ridges are labeled.

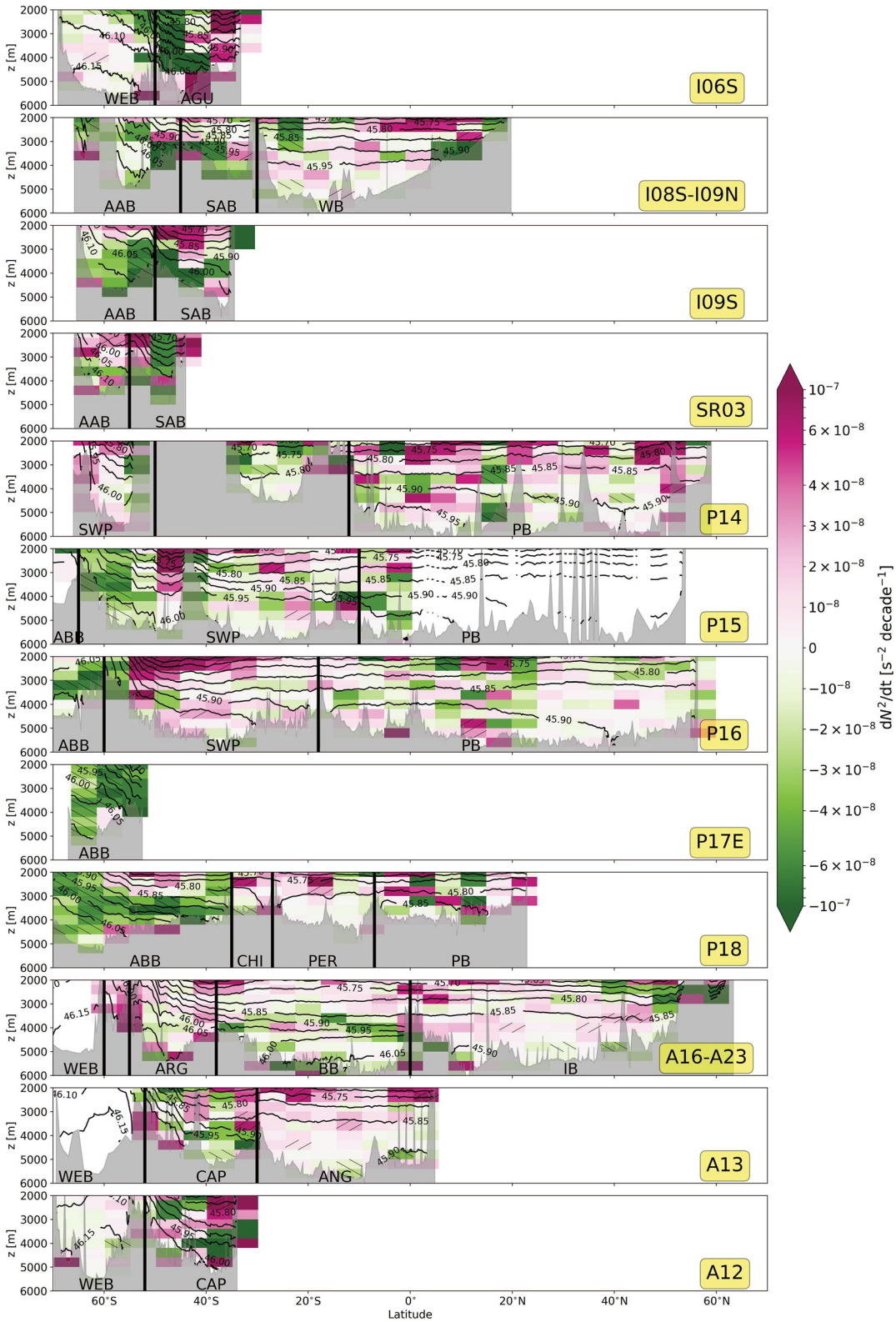

Figure 2. As in Figure 1b, but for dN^2/dt along meridional sections.

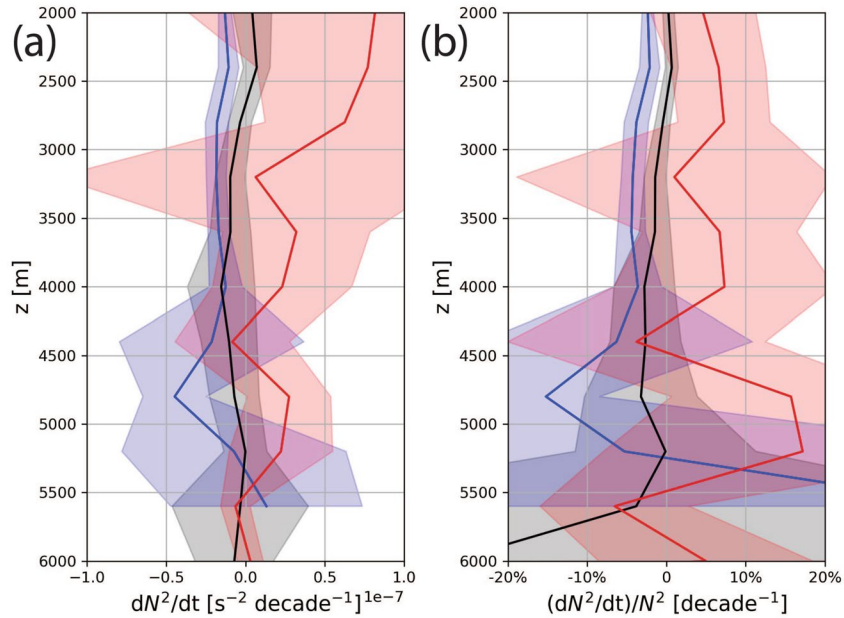

Figure 3. (a) Mean stratification trends dN^2/dt and (b) the mean percentage change of N^2 for the Northern Hemisphere (red), Southern Hemisphere (black), and regions south of 60°S (blue), with 95% confidence intervals (shaded).

(Figures S2 and S3 in Supporting Information S1). This signal is likely linked to the stratification change in the upper-layer AABW in the ABB.

In the Indian Ocean: The Ross-Adelie sourced AABW is mostly found in the eastern Indian Ocean basins while the Weddell-Enderby basin sourced AABW is observed in the western Indian Ocean basins (Solodoch et al., 2022). Decreasing stratification is found along the pathway of the Ross-Adelie sourced AABW in the AAB, in the South Australian basin (SAB), and in the southeastern part of the Wharton basin (see Figure S3b

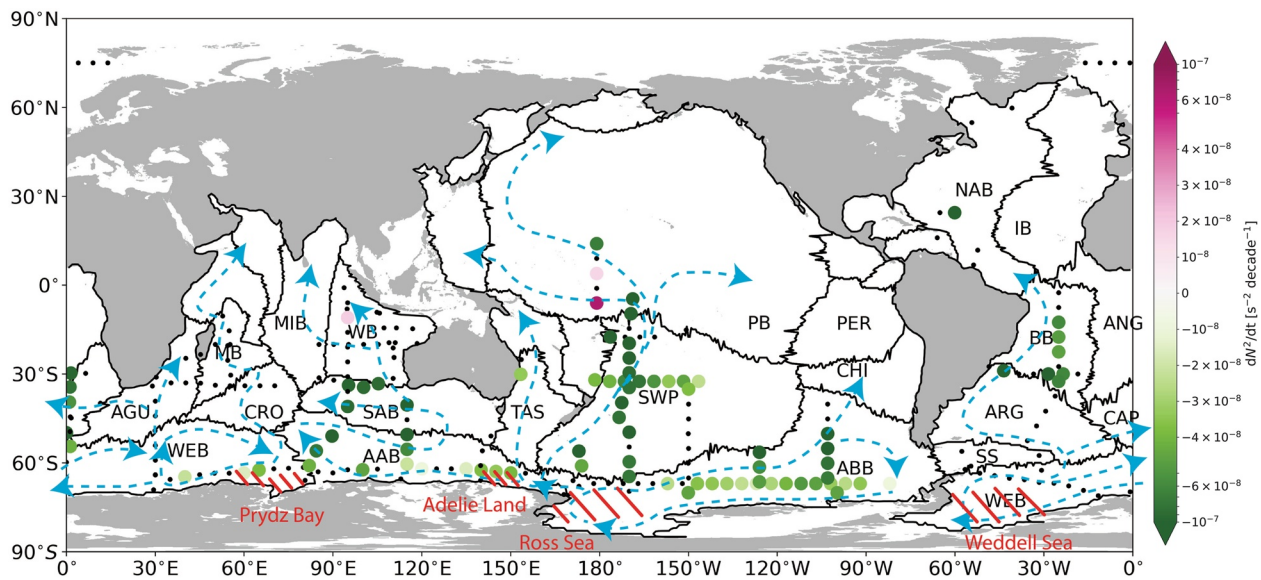

Figure 4. dN^2/dt averaged for σ_4 larger than 45.95 kg m^{-3}. Only results that are significantly different from zero at the 95% confidence level are shown. Black dots show locations of dN^2/dt estimated within 5° grids along repeat sections, where the bottom water is denser than σ_4 = 45.95 kg m^{-3}. Blue dashed arrows demark the pathways of the Antarctic-origin waters out of the Southern Ocean (pathway schematics adapted from Figure 3.3a in Lavin (2021) with simplification and details omitted). The four major Antarctica Bottom Water (AABW) formation regions are hatched in red. Note that there are two AABW formation regions in the WEB: the Weddell Sea and the Prydz Bay (Solodoch et al., 2022).

in Supporting Information S1). However, a similar signal is not observed in basins in the western Indian Ocean along the pathway of the Weddell-Enderby basin sourced AABW.

In the Atlantic Ocean: AABW from the Weddell Sea constitutes the Deep Western Boundary Current (DWBC) that flows along the continental slope of South America into the Argentine basin and then into the BB through the Vema and Hunter channels (Arhan et al., 1999; Reid, 1989). In the Argentine basin, no significant stratification changes in the AABW are detected along the combined section A16–A23. This is because the section crosses the Argentine basin in its central part and thus fails to sample the AABW carried by the DWBC. However, negative N^2 trends are found at the westernmost stations of section A10, just downstream of the main sill in the Vema channel. This signal of reduced stratification is detected both in Brazil and Cape basin, which seems to follow the pathway of the Weddell-Enderby basin sourced AABW.

While the AABW in its formation basins is continuously stratified throughout the deep and abyssal layers, sills between basins can block the densest upstream waters and result in nearly homogeneous abyssal layers in the downstream basin (Bryden & Nurser, 2003). This is because only the lighter AABW components overflow the sill and fill the abyss of the connecting basin with waters roughly of the density of the deepest isopycnal, which results in a weakly stratified abyssal layer below the sill depth (see schematic in Figure S6 in Supporting Information S1). In contrast, the stratified upper-layer AABW is not blocked by the sill and enters the basin unimpeded. While the overlying NADW is also weakly stratified, which is the case away from its origin, one can expect a stratified layer between the nearly homogenous NADW and abyssal layers in the downstream basin due to sill blockage. This feature was referred to as the "benthic thermocline" in the literature (e.g., Broecker et al., 1976; Chung, 1975; Reid, 1969), and has been observed both in the abyssal PB downstream of the Samoan Passage and in the abyssal BB downstream of the Vema Channel. Because of the sill blockage, decreased stratification primarily occurs at the "benthic thermocline" in the downstream basin. Our best-observed example of such a case is a band of negative N^2 trends along the combined section A16–A23 in the BB between the 45.85 and 45.95 kg m^{-3} isopycnals (Figure 2), with an average N^2 change of −12% per decade over the section between 40°S and the equator. For the case where there are no sills in passages or the sills are not tall enough to block the AABW, the "benthic thermocline" does not exist in the downstream basin. However, erosion of the densest isopycnals is commonly observed along the path of AABW. In this case, the vertical structure of stratification trends in the downstream basin generally follows the vertical structure in the upstream basin. One example is the bottom-reaching negative N^2 trend in the SAB downstream of the AAB (see along sections I08S–I09N and I09S in Figure 2).

4. Summary and Discussion

In this study we find that the stratification in both the deep (2,000–4,000 m) and abyssal (≥4,000 m) layers in the Southern Hemisphere oceans has decreased significantly since the 1990s, an observation that can be linked to the bottom intensified warming trend and/or freshening trend in deep and abyssal layers in many AABW formation regions. Averaged south of 60°S below 4,000 m, we find a mean trend of 6% per decade reduction in N^2. The decreasing stratification is found not only in the formation basins of AABW, but also in downstream basins along its path, and shows large spatial variability between basins. For example, significantly reduced stratification is found throughout the deep and abyssal layers both in Amundsen-Bellingshausen and AABs, while the layer average in the Weddell–Enderby basin does not significantly differ from zero. The large spatial variability in the Weddell–Enderby basin is due to the different responses of AABW formation to the changing climate in the two AABW formation regions in the basin. The vertical structure of the stratification trend in downstream basins is significantly impacted by the topography of the passages connecting basins. For the case where the AABW is partially blocked by sills in the passages, the upper-layer AABW enters the downstream basin and manifests a "benthic thermocline" between the weakly stratified abyssal layer and NADW layer. As a result, the decreasing stratification in such a downstream basin is mostly found at the "benthic thermocline." This is particularly clear in the "benthic thermocline" of the BB where our analysis reveals a N^2 trend of −12% per decade. This signal extends across the entire basin into the Fracture Zone valleys in the eastern BB where it likely affects the along-valley transport, upwelling, and diapycnal mixing processes (Clément & Thurnherr, 2018; Thurnherr et al., 2020; Zhao & Thurnherr, 2018). In contrast, where sills are absent or not tall enough to block the AABW, bottom-reaching negative N^2 trends are observed in the downstream basins (e.g., the SAB). In the Chile basin that is topographically separated from the ABB by tall ridges, dense AABW is mostly blocked from entering, and the observed negative N^2 trends are associated with the lightest AABW components.

Ocean stratification exerts influence on internal waves at all phases of their lifespan. For example, N is the upper frequency limit for freely propagating internal waves, it controls the vertical angle of internal waves of a given frequency (Gerkema & Zimmerman, 2008), it affects the locations where internal tidal beams are generated (Lien & Gregg, 2001), and it controls the amount of energy converted from the barotropic to internal tides (Jayne & St. Laurent, 2001; St. Laurent et al., 2002). Through modulating wave characteristics and processes, ocean stratification may eventually exert impacts on turbulence energy dissipation from breaking internal waves. As the turbulent buoyancy flux is closely related to both stratification and turbulence energy dissipation, the changing stratification in the deep and abyssal ocean has important implications for understanding the closure of the abyssal cell of the MOC. Furthermore, the changing stratification may directly impact the amount of abyssal waters that flow over sills and enter adjacent basins through hydraulic control. This has important implications for the diapycnal mixing in basins along the pathway of abyssal waters.

Although more accurate and comprehensive estimates await further investigation, below we use the turbulent diffusivity parameterization from Jayne and St. Laurent (2001) and a single-layer hydraulic model to give some rough estimates of the change of the turbulent buoyancy flux and overflow transport under a stratification reduction of 6%–15% per decade, which is taken from the mean and maximum of the N^2 trend below 4,000 m in regions south of 60°S. In the model of Jayne and St. Laurent (2001), the turbulent diffusivity due to breaking internal tides at topography can be parameterized as

$$\kappa_v = \frac{\Gamma q F(z)}{2N} k h^2 U^2, \tag{2}$$

where Γ represents the mixing efficiency (canonically assumed at a constant rate of 0.2), $q = 0.3 \pm 0.1$ is the inferred fraction of wave energy dissipated locally, $F(z)$ is the vertical structure function of the dissipation, k is the horizontal wavenumber, h is the topographic height, and U is the magnitude of the background barotropic tidal currents. Assuming all are unchanged except for N, a 6%–15% per decade reduction in N^2 corresponds to an increase in κ_v by 3%–7.5% per decade and a decrease in buoyancy flux $F_b = -\kappa_v N^2$ by 3%–7.5% per decade (see Supporting Information S1 for details). In a single-layer, non-rotating, inviscid hydraulic model, the volume flux of a hydraulically controlled overflow can be parameterized as

$$Q = \left(\frac{2}{3}\right)^{3/2} g'^{1/2} H^{3/2} L, \tag{3}$$

where L is the width of the sill, H is the depth difference between the flow's interface in the upstream basin and the sill, and g' is the reduced gravity (Pratt & Whitehead, 2007). Assuming H remains unchanged, and the reduction in N^2 corresponds to a 6%–15% reduction per decade in g', then we obtain a 3%–8% reduction per decade in the volume flux. A detailed analysis of the relationship between stratification, volume flux, and the level of the flow's interface (embedded in H for the simplified model) is beyond the scope of this work but will be given in another paper, where a continuously stratified hydraulic model will be used to evaluate the effect of decreasing N^2 in AABW.

Data Availability Statement

The GO-SHIP Easy Ocean data used for stratification calculation in the study is available at https://cchdo.ucsd.edu/products/goship-easyocean via https://doi.org/10.7942/GOSHIP-EasyOcean (Katsumata et al., 2022). The code used for calculating the N^2 trends and to produce all plots of this manuscript are freely available at the repository https://github.com/ShuwenTan-PO/N2change_EasyOcean.

Acknowledgments
This work was supported by the National Science Foundation under Grants U.S. GO-SHIP NSF OCE-1437015 and OCE-2023545. S. Tan acknowledges the support of the U.S. GO-SHIP Postdoctoral Fellowship augmented by LDEO institutional funding. The authors acknowledge the long-term efforts of the project PIs, cruise participants, ship officers, and crew members who helped collect, calibrate, and process the data. We thank the two anonymous reviewers for their constructive comments and suggestions.

References

Alford, M. H., Girton, J. B., Voet, G., Carter, G. S., Mickett, J. B., & Klymak, J. M. (2013). Turbulent mixing and hydraulic control of abyssal water in the Samoan passage. *Geophysical Research Letters*, *40*(17), 4668–4674. https://doi.org/10.1002/grl.50684

Arhan, M., Heywood, K. J., & King, B. A. (1999). The deep waters from the southern ocean at the entry to the argentine basin. *Deep Sea Research Part II: Topical Studies in Oceanography*, *46*(1–2), 475–499. https://doi.org/10.1016/S0967-0645(98)00110-6

Broecker, W., Takahashi, T., & Li, Y.-H. (1976). Hydrography of the central Atlantic—I. The two-degree discontinuity. *Deep-Sea Research and Oceanographic Abstracts*, *23*(12), 1083–1104. https://doi.org/10.1016/0011-7471(76)90886-X

Bryden, H. L., & Nurser, A. G. (2003). Effects of strait mixing on ocean stratification. *Journal of Physical Oceanography*, *33*(8), 1870–1872. https://doi.org/10.1175/1520-0485(2003)033⟨1870:EOSMOO⟩2.0.CO;2

Carter, G. S., Voet, G., Alford, M. H., Girton, J. B., Mickett, J. B., Klymak, J. M., et al. (2019). A spatial geography of abyssal turbulent mixing in the Samoan passage. *Oceanography*, *32*(4), 194–203. https://doi.org/10.5670/oceanog.2019.425

Chung, Y. (1975). Areal extent of the benthic front and variation of the scale height in Pacific deep and bottom waters. *Journal of Geophysical Research*, *80*(30), 4169–4178. https://doi.org/10.1029/JC080i030p04169

Clément, L., & Thurnherr, A. M. (2018). Abyssal upwelling in mid-ocean ridge fracture zones. *Geophysical Research Letters*, *45*(5), 2424–2432. https://doi.org/10.1002/2017GL075872

Clément, L., Thurnherr, A. M., & Laurent, L. C. S. (2017). Turbulent mixing in a deep fracture zone on the Mid-Atlantic Ridge. *Journal of Physical Oceanography*, *47*(8), 1873–1896. https://doi.org/10.1175/JPO-D-19-0021.1

Cusack, J. M., Voet, G., Alford, M. H., Girton, J. B., Carter, G. S., Pratt, L. J., et al. (2019). Persistent turbulence in the Samoan passage. *Journal of Physical Oceanography*, *49*(12), 3179–3197. https://doi.org/10.1175/JPO-D-19-0116.1

Desbruyères, D. G., McDonagh, E. L., King, B. A., & Thierry, V. (2017). Global and full-depth ocean temperature trends during the early twenty-first century from Argo and repeat hydrography. *Journal of Climate*, *30*(6), 1985–1997. https://doi.org/10.1175/JCLI-D-16-0396.1

Desbruyères, D. G., Purkey, S. G., McDonagh, E. L., Johnson, G. C., & King, B. A. (2016). Deep and abyssal ocean warming from 35 years of repeat hydrography. *Geophysical Research Letters*, *43*(19), 10–356. https://doi.org/10.1002/2016GL070413

Garrett, C., & Kunze, E. (2007). Internal tide generation in the deep ocean. *Annual Review of Fluid Mechanics*, *39*(1), 57–87. https://doi.org/10.1146/annurev.fluid.39.050905.110227

Gerkema, T., & Zimmerman, J. (2008). An introduction to internal waves. In *Lecture Notes, Royal NIOZ, Texel, 207*.

Gregg, M. C. (1989). Scaling turbulent dissipation in the thermocline. *Journal of Geophysical Research*, *94*(C7), 9686–9698. https://doi.org/10.1029/JC094iC07p09686

Hood, E., Sabine, C., & Sloyan, B. (2010). Go-ship repeat hydrography manual. Version 1: Cover page and contents (p. 3). https://doi.org/10.25607/OBP-833

Jayne, S. R., & St. Laurent, L. C. (2001). Parameterizing tidal dissipation over rough topography. *Geophysical Research Letters*, *28*(5), 811–814. https://doi.org/10.1029/2000GL012044

Johnson, G. C. (2008). Quantifying Antarctic bottom water and North Atlantic deep water volumes. *Journal of Geophysical Research*, *113*(C5), C05027. https://doi.org/10.1029/2007JC004477

Johnson, G. C., Cadot, C., Lyman, J. M., McTaggart, K. E., & Steffen, E. L. (2020). Antarctic bottom water warming in the Brazil basin: 1990s through 2020, from woce to deep argo. *Geophysical Research Letters*, *47*(18), e2020GL089191. https://doi.org/10.1029/2020GL089191

Johnson, G. C., Purkey, S. G., & Bullister, J. L. (2008). Warming and freshening in the abyssal southeastern Indian Ocean. *Journal of Climate*, *21*(20), 5351–5363. https://doi.org/10.1175/2008JCLI2384.1

Katsumata, K., Purkey, S. G., Cowley, R., Sloyan, B. M., Diggs, S. C., Moore, T. S., et al. (2022). Go-ship easy ocean: Gridded ship-based hydrographic section of temperature, salinity, and dissolved oxygen. *Scientific Data*, *9*(1), 1–8. https://doi.org/10.1038/s41597-022-01212-w

Lavin, P. D. (2021). *Innovative observational global and regional ocean water mass, circulation, and mixing analyses*. Ph.D. dissertation. University of Washington.

Legg, S. (2021). Mixing by oceanic lee waves. *Annual Review of Fluid Mechanics*, *53*(1), 173–201. https://doi.org/10.1146/annurev-fluid-051220-043904

Li, G., Cheng, L., Zhu, J., Trenberth, K. E., Mann, M. E., & Abraham, J. P. (2020). Increasing ocean stratification over the past half-century. *Nature Climate Change*, *10*(12), 1116–1123. https://doi.org/10.1038/s41558-020-00918-2

Lien, R.-C., & Gregg, M. (2001). Observations of turbulence in a tidal beam and across a coastal ridge. *Journal of Geophysical Research*, *106*(C3), 4575–4591. https://doi.org/10.1029/2000JC000351

MacKinnon, J. A., Zhao, Z., Whalen, C. B., Waterhouse, A. F., Trossman, D. S., Sun, O. M., et al. (2017). Climate process team on internal wave–driven ocean mixing. *Bulletin of the American Meteorological Society*, *98*(11), 2429–2454. https://doi.org/10.1175/BAMS-D-16-0030.1

Marshall, J., & Speer, K. (2012). Closure of the meridional overturning circulation through southern ocean upwelling. *Nature Geoscience*, *5*(3), 171–180. https://doi.org/10.1038/ngeo1391

McDougall, T. J., & Barker, P. M. (2011). Getting started with teos-10 and the Gibbs Seawater (GSW) oceanographic toolbox. *Scor/Iapso WG*, *127*(532), 1–28.

Menezes, V. V., Macdonald, A. M., & Schatzman, C. (2017). Accelerated freshening of Antarctic bottom water over the last decade in the southern Indian Ocean. *Science Advances*, *3*(1), e1601426. https://doi.org/10.1126/sciadv.1601426

Munk, W. H. (1966). Abyssal recipes. *Deep-Sea Research and Oceanographic Abstracts*, *13*(4), 707–730. https://doi.org/10.1016/0011-7471(66)90602-4

Munk, W. H., & Wunsch, C. (1998). Abyssal recipes II: Energetics of tidal and wind mixing. *Deep Sea Research Part I: Oceanographic Research Papers*, *45*(12), 1977–2010. https://doi.org/10.1016/S0967-0637(98)00070-3

Pratt, L. L., & Whitehead, J. A. (2007). *Rotating hydraulics: Nonlinear topographic effects in the ocean and atmosphere* (Vol. 36). Springer Science & Business Media. https://doi.org/10.1007/978-0-387-49572-9

Purkey, S. G., & Johnson, G. C. (2010). Warming of global abyssal and deep southern ocean waters between the 1990s and 2000s: Contributions to global heat and sea level rise budgets. *Journal of Climate*, *23*(23), 6336–6351. https://doi.org/10.1175/2010jcli3682.1

Purkey, S. G., & Johnson, G. C. (2012). Global contraction of Antarctic bottom water between the 1980s and 2000s. *Journal of Climate*, *25*(17), 5830–5844. https://doi.org/10.1175/JCLI-D-11-00612.1

Purkey, S. G., & Johnson, G. C. (2013). Antarctic bottom water warming and freshening: Contributions to sea level rise, ocean freshwater budgets, and global heat gain. *Journal of Climate*, *26*(16), 6105–6122. https://doi.org/10.1175/JCLI-D-12-00834.1

Purkey, S. G., Johnson, G. C., Talley, L. D., Sloyan, B. M., Wijffels, S. E., Smethie, W., et al. (2019). Unabated bottom water warming and freshening in the South Pacific Ocean. *Journal of Geophysical Research: Oceans*, *124*(3), 1778–1794. https://doi.org/10.1029/2018JC014775

Reid, J. L. (1969). Preliminary results of measurements of deep currents in the Pacific ocean. *Nature*, *221*(5183), 848. https://doi.org/10.1038/221848a0

Reid, J. L. (1989). On the total geostrophic circulation of the South Atlantic Ocean: Flow patterns, tracers, and transports. *Progress in Oceanography*, *23*(3), 149–244. https://doi.org/10.1016/0079-6611(89)90001-3

Solodoch, A., Stewart, A., Hogg, A. M., Morrison, A., Kiss, A., Thompson, A., et al. (2022). How does Antarctic bottom water cross the southern ocean? *Geophysical Research Letters*, *49*(7), e2021GL097211. https://doi.org/10.1029/2021GL097211

St. Laurent, L., Simmons, H., & Jayne, S. (2002). Estimating tidally driven mixing in the deep ocean. *Geophysical Research Letters*, *29*(23), 21-1–21-4. https://doi.org/10.1029/2002GL015633

Stommel, H., & Arons, A. (1959). On the abyssal circulation of the World Ocean—I. Stationary planetary flow patterns on a sphere. *Deep Sea Research*, *6*, 140–154. https://doi.org/10.1016/0146-6313(59)90065-6

Talley, L., Feely, R., Sloyan, B., Wanninkhof, R., Baringer, M., Bullister, J., et al. (2016). Changes in ocean heat, carbon content, and ventilation: A review of the first decade of go-ship global repeat hydrography. *Annual Review of Marine Science*, *8*(1), 185–215. https://doi.org/10.1146/annurev-marine-052915-100829

Tarakanov, R. Y., Morozov, E. G., & Frey, D. I. (2020). Hydraulic continuation of the abyssal flow from the vema channel in the southwestern part of the Brazil basin. *Journal of Geophysical Research: Oceans*, *125*(6), e2020JC016232. https://doi.org/10.1029/2020JC016232

Thurnherr, A. M., Clément, L., Laurent, L. S., Ferrari, R., & Ijichi, T. (2020). Transformation and upwelling of bottom water in fracture zone valleys. *Journal of Physical Oceanography*, *50*(3), 715–726. https://doi.org/10.1175/JPO-D-19-0021.1

Thurnherr, A. M., Laurent, L. C. S., Speer, K. G., Toole, J. M., & Ledwell, J. R. (2005). Mixing associated with sills in a canyon on the midocean ridge flank. *Journal of Physical Oceanography*, *35*(8), 1370–1381. https://doi.org/10.1175/JPO2773.1

van Wijk, E. M., & Rintoul, S. R. (2014). Freshening drives contraction of Antarctic bottom water in the Australian Antarctic basin. *Geophysical Research Letters*, *41*(5), 1657–1664. https://doi.org/10.1002/2013GL058921

Whalen, C. B., de Lavergne, C., Naveira Garabato, A. C., Klymak, J. M., MacKinnon, J. A., & Sheen, K. L. (2020). Internal wave-driven mixing: Governing processes and consequences for climate. *Nature Reviews Earth & Environment*, *1*(11), 606–621. https://doi.org/10.1038/s43017-020-0097-z

Whitehead, J. (1998). Topographic control of oceanic flows in deep passages and straits. *Reviews of Geophysics*, *36*(3), 423–440. https://doi.org/10.1029/98RG01014

Zhang, H. J., Whalen, C. B., Kumar, N., & Purkey, S. G. (2021). Decreased stratification in the abyssal southwest Pacific basin and implications for the energy budget. *Geophysical Research Letters*, *48*(19), e2021GL094322. https://doi.org/10.1029/2021GL094322

Zhao, J., & Thurnherr, A. M. (2018). Changes in bottom water physical properties above the Mid-Atlantic Ridge flank in the Brazil basin. *Journal of Geophysical Research: Oceans*, *123*(1), 708–719. https://doi.org/10.1002/2017JC013375